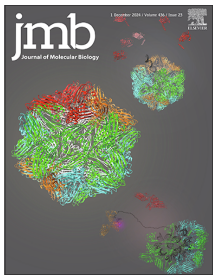

Regulated Proteolysis Induces Aberrant Phase Transition of Biomolecular Condensates into Aggregates: A Protective Role for the Chaperone Clusterin

Janine Kamps [1], Patricia Yuste-Checa [2], Fatemeh Mamashli [1], Matthias Schmitz [3], Maria Georgina Herrera [4], Susana Margarida da Silva Correia [3], Kalpshree Gogte [1], Verian Bader [4], Inga Zerr [3], F. Ulrich Hartl [2,5], Andreas Bracher [2], Konstanze F. Winklhofer [4,6], and Jörg Tatzelt [1,6*]

*1 - **Department Biochemistry of Neurodegenerative Diseases,** Institute of Biochemistry and Pathobiochemistry, Ruhr University, Bochum, Germany*
*2 - **Department of Cellular Biochemistry,** Max Planck Institute of Biochemistry, Martinsried, Germany*
*3 - **Department of Neurology,** University Medical Center, Göttingen, Germany*
*4 - **Department Molecular Cell Biology,** Institute of Biochemistry and Pathobiochemistry, Ruhr University, Bochum, Germany*
*5 - **Munich Cluster for Systems Neurology (SyNergy),** Munich, Germany*
*6 - **Cluster of Excellence RESOLV,** Bochum, Germany*

Correspondence to Jörg Tatzelt: *Ruhr University Bochum, Universitätsstr. 150, D-44801 Bochum, Germany. *Joerg.Tatzelt@rub.de* (J. Tatzelt)*
https://doi.org/10.1016/j.jmb.2024.168839
Edited by J. Buchner

Abstract

Several proteins associated with neurodegenerative diseases, such as the mammalian prion protein (PrP), undergo liquid–liquid phase separation (LLPS), which led to the hypothesis that condensates represent precursors in the formation of neurotoxic protein aggregates. However, the mechanisms that trigger aberrant phase separation are incompletely understood. In prion diseases, protease-resistant and infectious amyloid fibrils are composed of N-terminally truncated PrP, termed C2-PrP. C2-PrP is generated by regulated proteolysis (β-cleavage) of the cellular prion protein (PrP^C) specifically upon prion infection, suggesting that C2-PrP is a misfolding-prone substrate for the propagation of prions. Here we developed a novel assay to investigate the role of both LLPS and β-cleavage in the formation of C2-PrP aggregates. We show that β-cleavage induces the formation of C2-PrP aggregates, but only when full-length PrP had formed biomolecular condensates via LLPS before proteolysis. In contrast, C2-PrP remains soluble after β-cleavage of non-phase-separated PrP. To investigate whether extracellular molecular chaperones modulate LLPS of PrP and/or misfolding of C2-PrP, we focused on Clusterin. Clusterin does not inhibit LLPS of full-length PrP, however, it prevents aggregation of C2-PrP after β-cleavage of phase-separated PrP. Furthermore, Clusterin interferes with the *in vitro* amplification of infectious human prions isolated from Creutzfeldt-Jakob disease patients. Our study revealed that regulated proteolysis triggers aberrant phase transition of biomolecular condensates into aggregates and identified Clusterin as a component of the extracellular quality control pathway to prevent the formation and propagation of pathogenic PrP conformers.

Introduction

In prion diseases, such as Creutzfeldt-Jakob disease (CJD) in humans, the cellular mammalian prion protein (PrP^C) is converted into a misfolded isoform, designated scrapie prion protein (PrP^{Sc}). PrP^{Sc} forms partially protease-resistant protein aggregates and is the main component of infectious prions.[1] A considerable fraction of mature PrP^C is proteolytically processed *in vivo*, resulting in the formation of two distinct C-terminal fragments. One fragment, designated C1, is formed by α-cleavage of PrP^C under physiological conditions approximately at amino acid position 110. A second cleavage around amino acid position 90 (β-cleavage) is mainly observed under pathological conditions and generates C2-PrP.[2–7] Interestingly, a significant fraction of PrP^{Sc} present in the brains of terminally ill patients is made up of an N-terminally truncated fragment of PrP, designated C2-PrP^{Sc2} (Figure 1A). This observation suggests that β-cleavage of PrP^C may generate an aggregation-prone PrP fragment that serves as a preferred substrate for the propagation of infectious prions.[8] Like several other proteins associated with neurodegenerative diseases, PrP undergoes liquid–liquid phase separation (LLPS) to form biomolecular condensates.[9–17] Therefore, it has been proposed that aberrant liquid–solid phase separation of biomolecular condensates could promote formation of neurotoxic protein aggregates.[18–21] However, it has also been shown that solid aggregates can form independently of biomolecular condensates.[22–25]

Phase separation can be regulated by post-translational modifications (PTMs) and chaperones.[26,27] With regard to PrP, the chaperone Clusterin (also known as ApoJ) is of particular interest. Like PrP it is localized in the extracellular space, inhibits protein aggregation in an ATP-independent manner and plays a role in the pathogenesis of Alzheimer's disease and prion diseases. It is note-

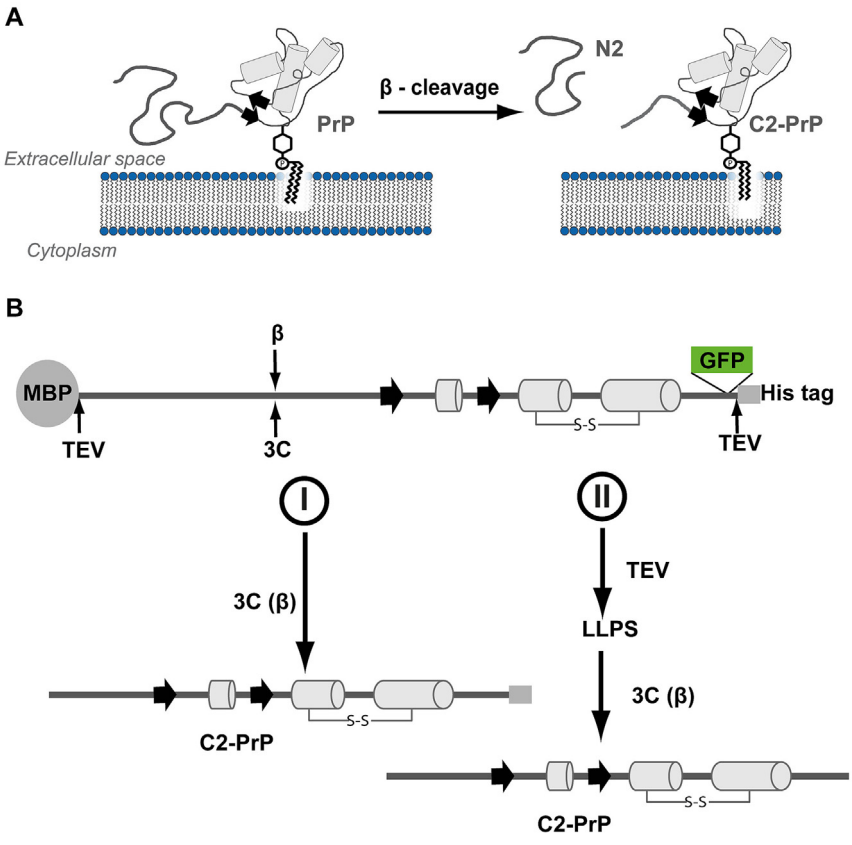

Figure 1. Schematic representations of proteolytic processing of the prion protein *in vivo* and *in vitro*. (A) PrP cleavage at the plasma membrane. β-cleavage: site that generates the N2 and C2 fragments. **(B)** Scheme of the recombinant fusion protein and the experimental approaches. Release of the N-terminal maltose-binding protein (MBP) and the C-terminal His tag (6xHis) was mediated by TEV protease cleavage. The β-cleavage was induced by PreScission (3C) protease. The fusion protein was expressed either with or without GFP at the C-terminus. C2-PrP was generated via two routes. I) β-cleavage was induced directly from the soluble PrP. II) Firstly, LLPS of PrP was initiated by TEV protease incubation. Secondly, β-cleavage was induced in the condensate state of PrP.

worthy that, in addition to its functions as an extracellular chaperone, Clusterin has been proposed to act in a wide variety of other roles, including the promotion of cell survival, sperm maturation, complement inhibition, and cell differentiation.[28,29–40]

Reversible PTMs, such as methylation,[41] phosphorylation,[42] acetylation,[43] ubiquitylation,[44,45] SUMOylation[46] and PARylation,[47] have been described to modulate LLPS and protein aggregation. Whether regulated proteolysis plays a role in the regulation of phase transitions is not yet known. Using a novel *in vitro* model, we demonstrate a context-specific activity of regulated proteolysis to promote the rapid transition of liquid–liquid phase-separated PrP into aggregates. In addition, our findings reveal an activity of the chaperone Clusterin to specifically inhibit protein aggregation without affecting liquid–liquid phase separation.

Results and Discussion

An in vitro approach to study β-cleavage of PrP before and after LLPS

We have established *in vitro* models to analyze liquid–liquid phase separation of PrP.[14,16,17,48,49] The assay uses PrP fusion proteins with an N-terminal maltose-binding protein (MBP) to keep the recombinant PrP soluble during expression and purification, and a C-terminal His-tag for affinity purification. LLPS of PrP is initiated by cleaving MBP with tobacco etch virus (TEV) protease and analyzed by laser scanning microscopy. To investigate the potential effect of β-cleavage on phase separation of PrP, we inserted a PreScission (3C) protease cleavage site between amino acids 89 and 90 of PrP. This construct allows us to analyze formation of C2-PrP via two different pathways (Figure 1B). In pathway I, C2-PrP is generated directly by cleavage of non-phase-separated MBP-PrP with 3C protease. In pathway II, we first cut off MBP with TEV protease to initiate LLPS of full-length PrP. 3C protease is then added to the biomolecular condensates to generate C2-PrP from phase-separated PrP.

β-cleavage of liquid–liquid phase-separated PrP triggers formation of C2-PrP aggregates

First, we generated C2-PrP-GFP directly from non-phase-separated MBP-PrP-GFP by incubating the recombinant protein with 3C protease (pathway I). The evenly distributed GFP fluorescence indicated that MBP-PrP-GFP was soluble after purification from *E. coli* (Figure 2A, I). Similarly, C2-PrP-GFP generated by β-cleavage of MBP-PrP-GFP remained soluble (Figure 2A, I, 3C (β)), corroborating earlier results that C2-PrP does not undergo LLPS under these conditions.[9,14] Analysis of the samples by SDS-PAGE and Coomassie brilliant blue staining confirmed that C2-PrP-GFP was efficiently generated by 3C protease-mediated processing (Figure S1A). Following pathway II, we first induced LLPS of full-length PrP-GFP by releasing the MBP tag with TEV protease, resulting in the formation of PrP assemblies (Figure 2A, II, TEV). Fluorescence recovery after photobleaching (FRAP) recordings proved that the full-length PrP-GFP molecules in the assemblies were highly dynamic, characteristic of the liquid-like state of condensates (Figure 2A). Furthermore, the assemblies fused, thus providing additional evidence of LLPS (Figure S1B). We then added 3C protease to the condensates composed of full-length PrP to generate C2-PrP via β-cleavage. Since C2-PrP-GFP did not undergo phase separation when generated directly from MBP-PrP-GFP, we expected that β-cleavage would reverse PrP condensate formation, resulting in soluble C2-PrP-GFP. Unexpectedly, the liquid-like assemblies of full-length PrP-GFP changed their morphology after β-cleavage and started to form irregularly shaped clusters (Figure 2A, II, 3C (β)). FRAP recordings revealed that C2-PrP-GFP within these assemblies was immobile, indicating that β-cleavage of liquid–liquid phase-separated full-length PrP had triggered the formation of C2-PrP aggregates. To exclude the possibility that the GFP tag influences phase transition, the same set of experiments was conducted with MBP-PrP fusion proteins devoid of the C-terminal GFP. Images taken by bright-field microscopy confirmed that C2-PrP generated from non-phase-separated PrP remained soluble (Figure 2B, I; Figure S1C), whereas β-cleavage of liquid–liquid phase-separated PrP induced the formation of C2-PrP assemblies with irregular structures (Figure 2B, II; Figure S1C). To gain further insight into the material properties of the C2-PrP aggregates we analyzed whether it would bind Thioflavin T (ThT), which is used as an indicator of amyloid-like structure.[50] However, no significant increase in ThT fluorescence was observed following 3C protease-induced aggregation (Figure S1D).

In conclusion, our newly developed *in vitro* model is suitable for comparing the impact of β-cleavage on non-phase-separated PrP or on PrP following the formation of biomolecular condensates by LLPS. Intriguingly, β-cleavage of full-length PrP promotes aggregation of C2-PrP, but only when full-length PrP is in a liquid-like condensate state prior to proteolysis. Most likely, upon removal of the intrinsically disordered N-terminal N2 domain hydrophobic interactions dominate and lead to aggregation of C2-PrP due to its high concentration in the dense phase of the condensates. Alternatively, a particular spatial arrangement of the PrP molecules in the condensates may predispose C2-PrP to hydrophobic interactions after removal of the N-terminal domain.

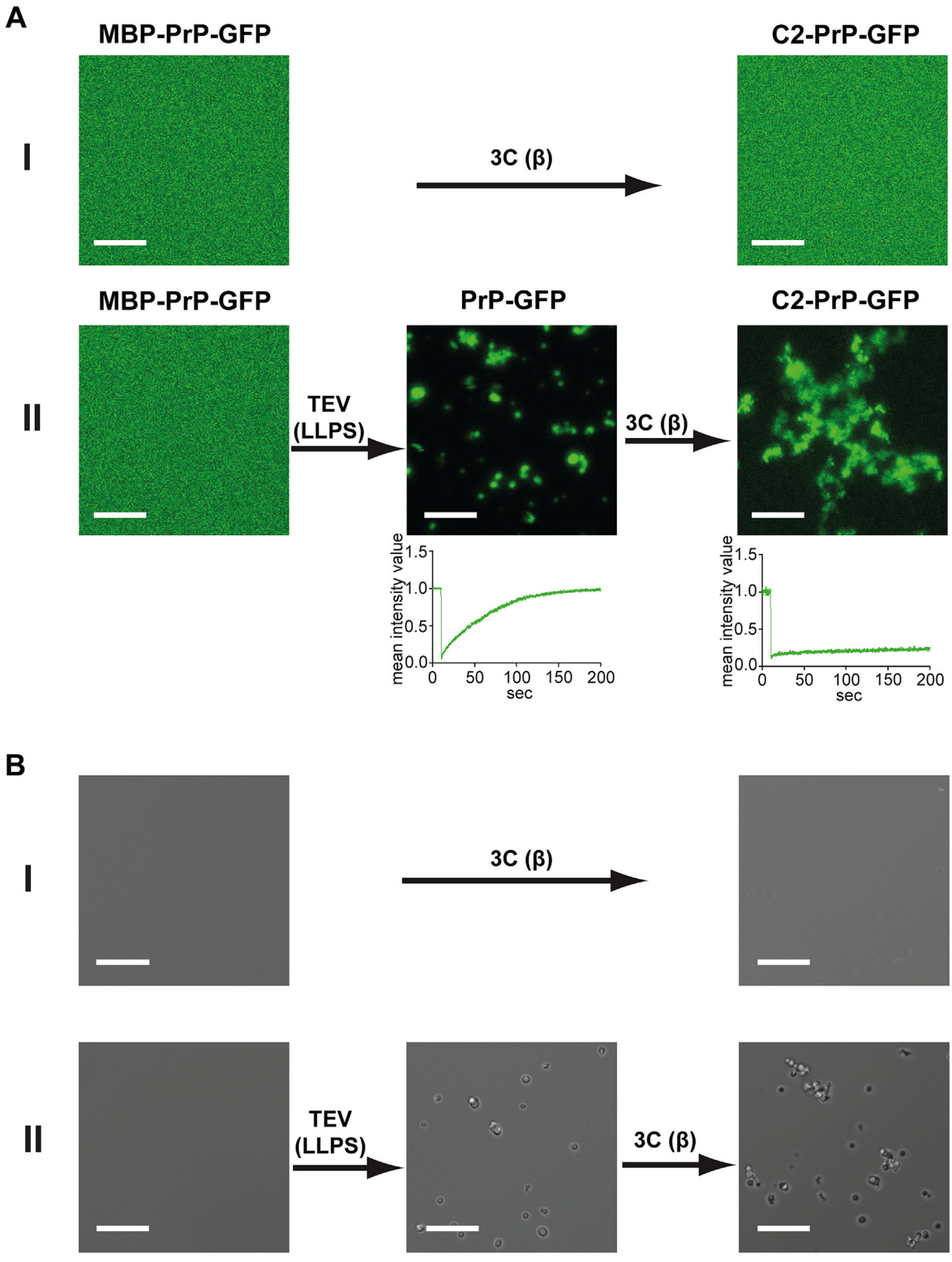

Figure 2. Proteolytic processing of liquid–liquid phase-separated prion protein induces protein aggregates. (A) MBP-PrP-GFP (10 μM in 10 mM Tris pH 7.4) was incubated for 2 h with 3C protease (I), or first for 1 h with TEV protease and then for an additional 1 h with 3C protease (II). The samples were analyzed by laser scanning microscopy (scale bar, 10 μm). Protein mobility within the PrP assemblies was measured by fluorescence recovery after photobleaching (FRAP). After 10 s of baseline recording (pre-bleach), a small area of interest (AOI) was photobleached. The average normalized fluorescence intensity of three AOIs was plotted over time. **(B)** MBP-PrP (10 μM in 10 mM Tris pH 7.4) was incubated for 2 h with 3C protease (I), or first for 1 h with TEV protease and then for an additional 1 h with 3C protease (II). The samples were analyzed by bright-field microscopy (scale bar, 10 μm).

The extracellular chaperone Clusterin prevents formation of C2-PrP aggregates after β-cleavage

We have previously shown that the chaperone Clusterin alleviates the toxic effect of PrP^{Sc} in cellular models.[51] Thus, we were wondering whether Clusterin also modulates LLPS or LSPS of PrP. We mixed MBP-PrP-GFP with increasing amounts of recombinant Clusterin and then induced LLPS by TEV protease-mediated cleavage. At a ratio of up to 1:1, PrP-GFP still formed condensates analogous to the sample without Clusterin, indicating that Clusterin did not interfere with LLPS of PrP (Figure 3A, +TEV).

When we added 3C protease to the mixture of phase-separated full-length PrP and Clusterin to induce β-cleavage of PrP, Clusterin prevented the transition of PrP-GFP condensates to C2-PrP-GFP aggregates. Instead, C2-PrP-GFP was now in a non-phase-separated soluble state (Figure 3A + 3C(β)). The inhibitory effect of Clusterin was already seen at a ratio of 10:1 (PrP: Clusterin), corroborating earlier findings that Clusterin can prevent protein aggregation under sub-stoichiometric conditions.[52] To confirm that Clusterin did not interfere with TEV protease or 3C protease-mediated processing the samples were analyzed by SDS-PAGE and Coomassie brilliant blue staining (Figure S2A). When Clusterin was added after C2-PrP-GFP aggregates have been formed from liquid-liquid phase-separated PrP by β-cleavage, Clusterin had no apparent effect on the aggregates. Thus, Clusterin is not able to dissolve preformed C2-PrP-GFP aggregates (Figure 3B).

To study the interaction of Clusterin with PrP, we employed Clusterin fluorescently labeled with Alexa Fluor 594 (A594). First, we mixed A594-Clusterin with MBP-PrP-GFP and then induced LLPS by adding TEV protease. This approach demonstrated that Clusterin is present in the biomolecular condensates formed by PrP-GFP via LLPS, indicating an interaction of the chaperone with soluble PrP prior to its aggregation (Figure 4A, upper row). A594-Clusterin did also interact with preformed C2-PrP-GFP aggregates, but as shown above with unlabeled Clusterin, did not dissolve the aggregates (Figure 4A, lower row).

The pronounced activity of Clusterin raised the question of whether other chaperones would have similar effects on PrP LLPS and C2-PrP aggregation. To address this issue, we tested alpha-Crystallin B and Hsc70. Similar to Clusterin, alpha-Crystallin B and Hsc70 did not interfere with LLPS of full-length PrP. However, under conditions where Clusterin was effective in keeping C2-PrP soluble, neither of the other two chaperones inhibited C2-PrP-GFP aggregation (Figure S2B).

In summary, our experiments showed distinct activities of Clusterin on phase transitions. While the chaperone did not interfere with LLPS of PrP it prevented LSPS and thereby the formation of PrP aggregates. Consistent with previous findings that Clusterin acts as an ATP-independent holdase,[31,53] preformed C2-PrP aggregates were not dissolved by Clusterin. The recruitment of Clusterin into the condensates formed by PrP via LLPS was an interesting observation. It indicated an interaction between Clusterin and soluble PrP prior to onset of aggregation. This finding is in line with the activity of Clusterin to associate with native PrP^{C} in cultured cells and in the mouse brain.[54,55]

Clusterin inhibits PrP^{Sc}-induced conversion of soluble PrP into amyloid fibrils

In prion diseases PrP^{Sc} replicates by binding to PrP^{C} and catalyzing its conversion into PrP^{Sc}.[56] To explore a possible activity of Clusterin to mitigate the propagation of PrP^{Sc}, we utilized the real-time quaking-induced conversion (RT-QuIC) assay. RT-QuIC mimics the seeded conversion process of soluble PrP^{C} into amyloid by infectious prions.[57] During the reaction, small quantities of infectious PrP^{Sc} isolated from CJD patients bind to and convert soluble recombinant PrP molecules into amyloid fibrils. The newly formed amyloid is quantified by a ThT dye fluorescence assay (Figure S2C). We performed the RT-QuIC with cerebrospinal fluid (CSF) from CJD patients in the presence or absence of recombinant Clusterin. Indeed, Clusterin efficiently prevented the formation of ThT-positive aggregates, whereas BSA, used as a control, had no inhibitory effect (Figs. 4B).

Our study demonstrates that regulated proteolysis of PrP can initiate an aberrant phase transition of biomolecular condensates into protein aggregates and suggests that β-cleavage of PrP^{C}, which occurs in prion diseases, may contribute to the formation of scrapie prions (Figure 4C). This provides a mechanistic basis for the observation that inhibiting β-cleavage of PrP^{C} in scrapie-infected cultured cells reduces the amount of PK-resistant PrP^{Sc}.[8] Moreover, our data showing that Clusterin inhibits propagation of scrapie prions *in vitro* provides an explanation for the shortened incubation time observed in prion-infected Clusterin knockout mice.[40]

The discovery that proteolytic processing of liquid–liquid phase-separated proteins can induce their transition into aggregates may have broader implications, as pathological protein deposits found in other neurodegenerative diseases are also formed by proteolytic fragments. Examples include the fragments of TDP-43 in FTLD and ALS,[58] α-synuclein in Parkinson's disease,[59] and mutant huntingtin in Huntington's disease.[60] Since the physiological conformers of the corresponding full-length proteins have the propensity to undergo LLPS, it will be interesting to test whether proteolytic processing of those proteins within condensates also promote protein aggregation.

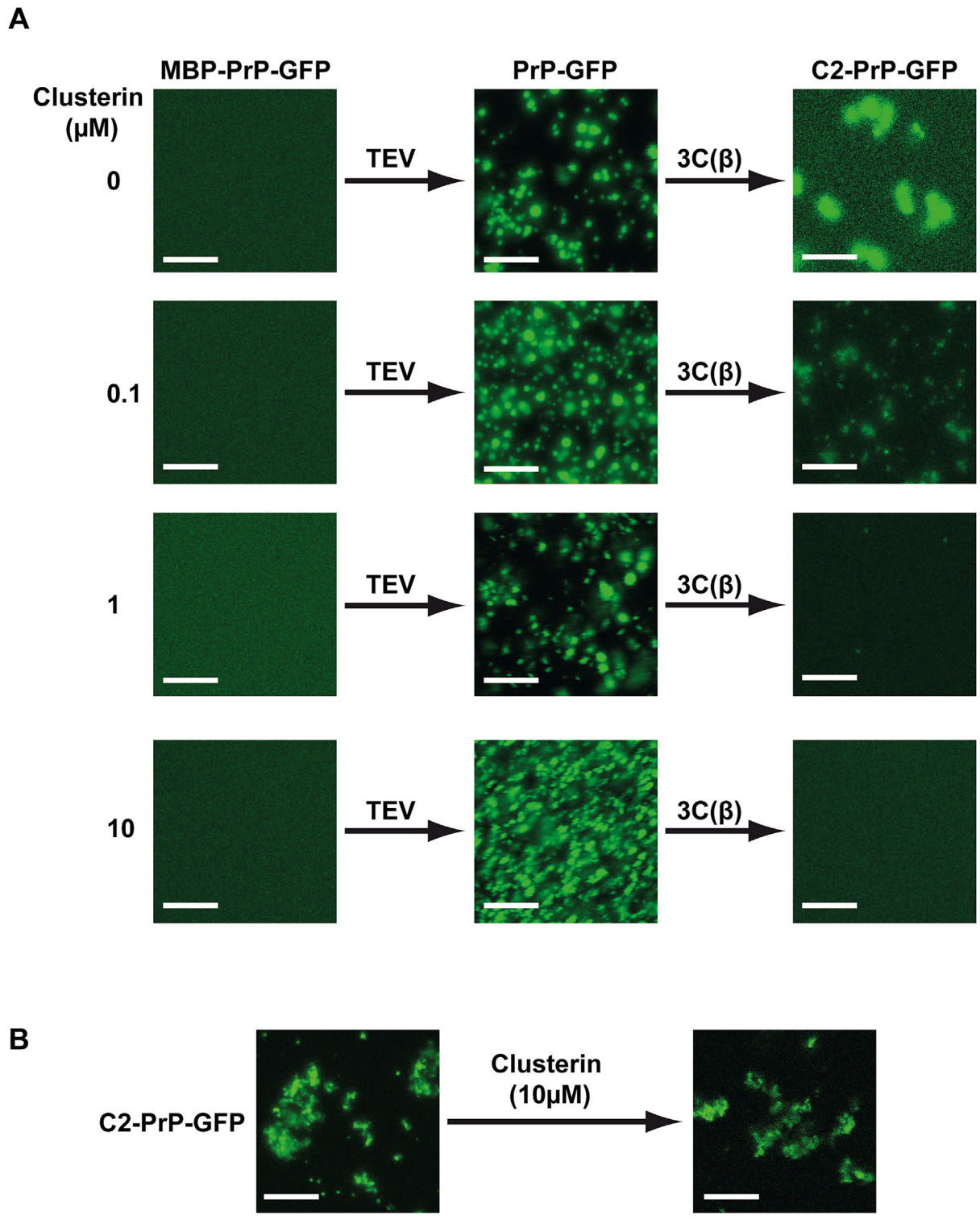

Figure 3. The chaperone Clusterin prevents transition of liquid–liquid phase-separated PrP into aggregates. **(A)** MBP-PrP-GFP (10 μM in 10 mM Tris pH 7.4) and Clusterin were incubated for 1 h at the indicated concentrations with TEV protease, followed by a further 1 h with 3C protease. The samples were analyzed by fluorescence microscopy (scale bar, 10 μm). **(B)** MBP-PrP-GFP (10 μM in 10 mM Tris pH 7.4) was incubated for 1 h with TEV protease and then for additional 1 h with 3C protease. To the sample containing C2-PrP-GFP assemblies, Clusterin (10 μM in 10 mM Tris pH 7.4) was added for 1 h. Phase separation was analyzed by fluorescence microscopy (scale bar, 10 μm).

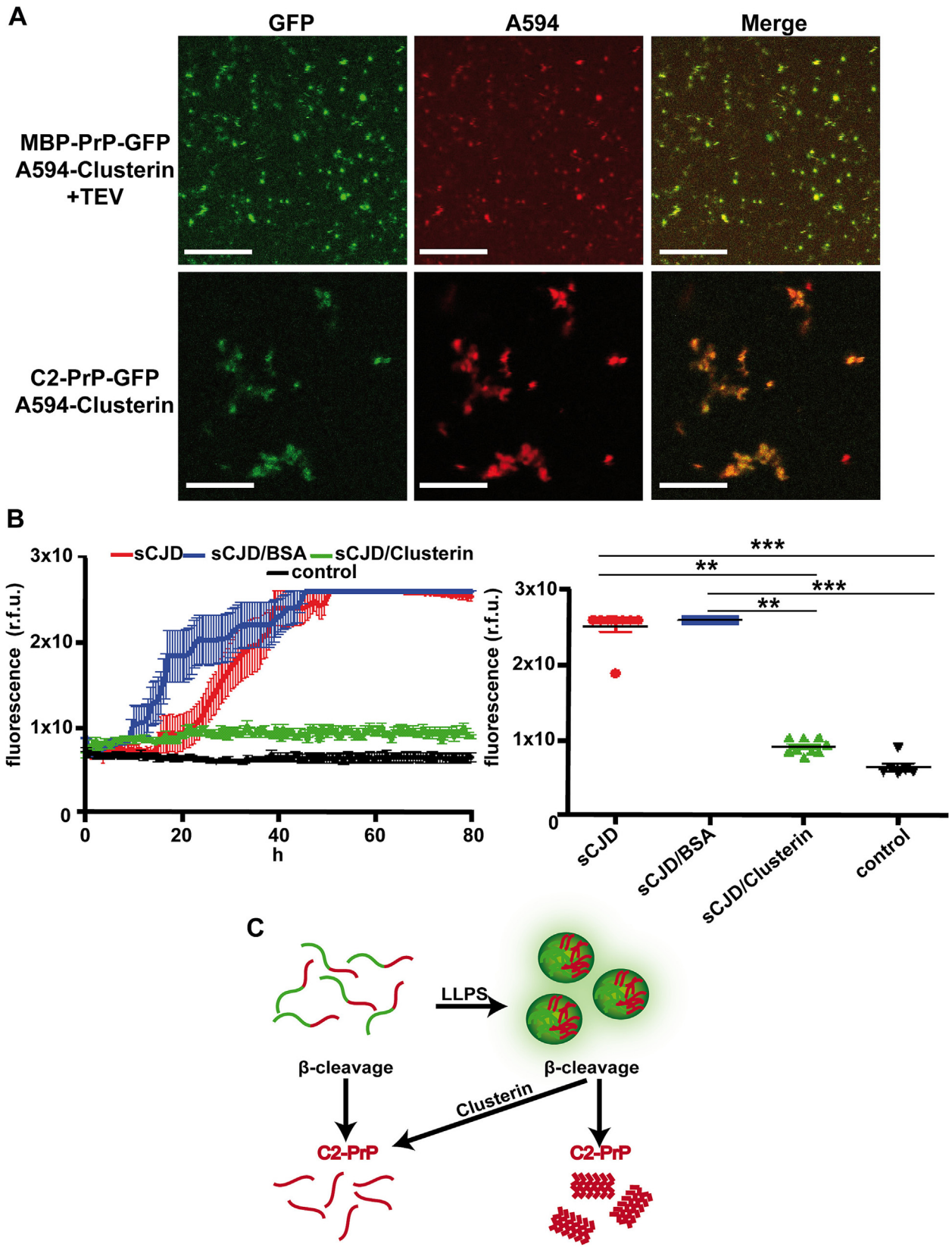
A
GFP
A594
Merge
MBP-PrP-GFP
A594-Clusterin
+TEV
C2-PrP-GFP
A594-Clusterin
B
sCJD
sCJD/BSA
sCJD/Clusterin
control
fluorescence (r.f.u.)
3x10
2x10
1x10
0
0
20
40
60
80
h
***
**
***
**
sCJD
sCJD/BSA
sCJD/Clusterin
control
C
LLPS
β-cleavage
β-cleavage
Clusterin
C2-PrP
C2-PrP

Material and Methods

Plasmids/constructs

The plasmid of PrP with a PreScission protease (3C) insertion between amino acids 89 and 90 is based on the coding region of mouse PrP gene (Prnp, GenBank accession number **M18070**) modified to express PrP-L108M/V111M for mAb 3F4 detection. The insertion of the 3C cleavage sequence was performed by overlap PCR technique. To generate the MBP-PrP3C89.90-eGFP-TEV-His_6 and MBP-PrP3C89.90-TEV-His_6 constructs, we exchanged the PrP coding region from the vector with the desired constructs from the plasmids previously described (Kamps *et al*, 2021). The amplification and maintenance of the plasmids was performed in *Escherichia coli* TOP10 (Thermo Fisher Scientific). The plasmid of Clusterin is based on the DNA sequence from human embryonic kidney 293T (HEK293T) cells and was inserted into a pB-T-PAF vector. The resulting plasmid was designated pB-T-PAF-Clu.

Protein expression and purification

Protein expression and purification was performed as previously described.[14] Briefly, MBP-PrP3C89.90-eGFP-TEV-His_6 and MBP-PrP3C89.90-TEV-His_6 were transformed into Origami™ B (DE3) competent cells (Novagen). Afterwards, 1L of lysogeny broth medium was inoculated and grown to an absorbance (600 nm) of 0.9. Expression was induced with 0.5 mM IPTG and incubated overnight at 25 °C, 120 rpm. Next the bacteria were harvested (5,000g, 4 °C, 20 min), the pellet was washed with 20 mL Millipore water, centrifuged (2,000*g*, 4 °C, 20 min) and stored at −20 °C until further use. Purification was started with pellet resuspension in lysis buffer (50 mM Na_2HPO_4/NaH_2PO_4 (pH 8.0), 500 mM NaCl, 0.01 mM $ZnCl_2$, 10% glycerol). SLM AMINCO French Press (Thermo Fisher Scientific) was used for protein lysis. Then the protein solution was centrifuged again (40,000*g*, 45 min, 4 °C). His-Trap FF column (GE Healthcare) was equilibrated with lysis buffer, protein was loaded and washed first with five CV lysis buffer containing 20 mM imidazole and second washed with three CV lysis buffer containing 50 mM imidazole. Elution was initiated by lysis buffer containing 200 mM imidazole. The eluted protein was dialyzed overnight in dialysis buffer (50 mM Na_2HPO_4/NaH_2PO_4 (pH 8.0), 500 mM NaCl, 0.01 mM $ZnCl_2$, 5% glycerol). Protein concentrations were calculated by measuring the absorbance at 280 nm by NanoDrop 2000 (Thermo Scientific) and using the corresponding extinction coefficients for MBP-PrP-3C89.90-eGFP-TEV-His6 (ε280nm = 154840 M^{-1} cm^{-1}), MBP-PrP3C89.90-TEV-His6(ε 280nm = 132825 M^{-1} cm^{-1}) and Clusterin (ε280nm = 39015 M^{-1} cm^{-1}). The proteins were aliquoted and stored at − 80 °C. WT Clusterin was expressed and purified as previously described.[34] In brief, the recombinant protein was expressed for four days by HEK293E-CluStrep cells, which were cultured in FreeStyle 293 Expression Medium (Thermo Fisher Scientific). Clusterin was secreted by the cells and the cell culture supernatant was harvested and separated from the HEK293E-Clu cells by centrifugation. Before purification, the medium was dialyzed to the wash buffer (20 mM Na acetate pH 5.0). Afterwards the dialyzed medium was centrifuged to remove possible precipitates and loaded onto HiTrap SP XL cation exchange column previously equilibrated with wash buffer. The column was washed with five CV wash buffer. Subsequently, Clusterin was eluted with a 0–500 mM linear NaCl gradient. Eluates were analyzed and Clusterin containing fractions were pooled. Purification was continued via size exclusion chromatography. Superdex-200 equilibrated with 20 mM Na acetate pH 5.0, 100 mM NaCl, 1 mM EDTA was loaded with clusterin containing fractions. Fractions were again analyzed for pure clusterin, pooled and concentrated to a desired concentration by Vivaspin 500 columns (Sartorius Stedim biotech) with 10-kDa molecular weight cut off. Protein concentration was determined by NanoDrop 2000 (Thermo Scientific), aliquoted and stored at −80 °C. Hsc70 was

Figure 4. Clusterin inhibits PrP scrapie fibril formation generated from CSF of Creutzfeldt-Jacob disease (CJD) patients. (A) MBP-PrP-GFP (10 μM in 10 mM Tris pH 7.4) and A594-labeled Clusterin (10 μM) were mixed and incubated for 1 h with TEV protease and then analyzed by fluorescence microscopy (scale bar, 10 μm; upper row). Preformed C2-PrP-GFP aggregates (10 μM in 10 mM Tris pH 7.4) were incubated with A594-labeled Clusterin (10 μM) and then analyzed by fluorescence microscopy (scale bar, 10 μm; lower row). **(B)** 15 μL CSF of three different CJD patients and two control patients were analyzed. Statistical analysis of the ThT assay results at timepoint 50 h (right panel). The graph displays the mean plus/minus the SEM from n = 6–9 after 50 h. After performing a Kolmogorov-Smirnov test to test for gaussian distribution, a non-parametric Kruskal-Wallis test followed by a Dunn's multiple comparison test was performed, $^{**}p < 0.01$, $^{***}p < 0.001$. **(C)** Schematic summary of the findings. Removal of the intrinsically discorded N-terminal fragment (green) by β-cleavage of non-phase separated full length PrP results in the formation of soluble C2-PrP (red). In contrast, C2-PrP (red) forms aggregates if PrP underwent LLPS prior to β-cleavage. Aggregation of C2-PrP is prevented by the chaperone Clusterin.

expressed and purified as described.[61] Alpha-Crystallin B was purchased from Prospec (Cat# HSP-003).

Clusterin labeling

Clusterin was labeled with Alexa594 N-hydroxysuccinimide ester (Thermo Fisher Scientific). Before labeling, Clusterin buffer was exchanged to 0.1 M sodium bicarbonate buffer pH 8.3 (N-terminal labeling buffer) using a Nap5 column. Labeling was subsequently performed at a 4-fold molar excess of Alexa 594 for 1.5 h at room temperature. Free dye was removed using a Nap5 column, pre-equilibrated with PBS buffer.

Sample preparation

Aliquots of the respective proteins were thawed on ice. The buffer was exchanged to 10 mM Tris, pH 7.4 using Vivaspin 500 columns (Sartorius Stedim biotech) with 30-kDa or 10-kDa molecular weight cut off. After buffer exchange the solution was centrifuged at 20,000*g*, at 4 °C for 10 min to remove possible aggregates. The final protein concentration was determined by NanoDrop 2000. To induce LLPS, the protein solution was incubated with TEV protease (2.7 μM) for 2 h to release the MBP and His Tag. β-cleavage was initiated by incubation with 3C protease (2.2 μM) for 2 h. In the experiments with labeled Clusterin, 5 μM Alexa Fluor 594 (A594) labeled Clusterin was mixed with 5 μM unlabeled Clusterin.

Laser scanning microscopy and FRAP recording

Fluorescent imaging laser scanning microscopy was performed as described.[14,62] An ELYRA PS.1 (Carl Zeiss) microscope with an imaging detector (LSM 880; Carl Zeiss) was used. The 63× numerical aperture 1.4 oil-immersion objective was chosen to record a z-stack of 67.5 × 67.5 × 10 μm and 0.900 μm for each optical section. The power of the argon laser was set to 0.006% at 488 nm with pixel dwell time of 5.71 μs. These settings were kept constant during all measurements. The Plan-Apochromat 100x numerical aperture 1.46 oil differential interference contrast M27 objective and ZEN2.1 bleaching and region software module was used for FRAP experiments. Three circular regions with a 12-pixel diameter were selected as regions of interest. Two regions were used as background signal and reference signal. The other region was bleached with 100% laser power and a pixel dwell time of 8.71 ms, with scan time of 111.29 ms and pixel dwell time of 1.61 ms. Excel 2016 was used for data evaluation and diagrams were performed in GraphPad Prism.

Thioflavin-T fluorescence measurement

To samples containing liquid–liquid phase-separated PrP (+TEV) or aggregated C2-PrP (+TEV, +3C) Thioflavin-T was added (final concentration 25 μM) and fluorescence intensity was measured with a BioTek CYTATION 5 using the excitation and emission wavelengths of 450 and 500 nm, respectively. For comparison, the Thioflavin-T fluorescence intensity of α-synuclein preformed fibrils (PFFs) were measured in parallel. The αSyn-PFFs were prepared as described previously.[63]

RT-QuIC assay

The RT-QuIC assay was performed as previously described.[64,65] In brief, 15 μL of cerebrospinal fluid (CSF) was added to 85 μL reaction buffer (5xPBS (pH 6.9), 170 mM NaCl, 1 mM EDTA, 10 μM Thioflavin-T) containing 0.1 mg/mL recombinant PrP (Thermo Fisher Scientific/Prionics). All RT-QuIC experiments were performed using a chimeric recombinant PrP composed of Syrian hamster PrP (residues 14–128) followed by sheep PrP (residues 141–234 of the R154 Q171 polymorph [GenBank accession number **AY907689**]) as described before.[66] This chimeric PrP is less prone to self-aggregation, which can lead to false-positive RT-QuIC reactions. Each patient sample was analyzed in triplicate. Clusterin and BSA was added directly into the reaction mix. The prepared plates were securely sealed with Nunc/Sigma Aldrich sealing tape and subjected to incubation in a FLUO Star OMEGA plate reader (BMG Labtech) at 42 °C for 80 h, involving intermittent quaking cycles. These cycles comprised one-minute double-orbital quaking at 600 rpm, followed by a one-minute incubation break. The kinetics of β-sheet formation were assessed by monitoring ThT fluorescence signals (excitation at 450 nm and emission at 480 nm) at 30 min intervals, measured in relative fluorescence units (r.f.u.).

Ethics statement

The study was conducted according to the revised Declaration of Helsinki and Good Clinical Practice guidelines. It has been approved by the local ethic committee at the University Medical Center Goettingen (Goettingen, Germany) (No. 9/6/0). Informed consent was given by all study participants or their legal next of kin.

CRediT authorship contribution statement

Janine Kamps: Writing – review & editing, Methodology, Investigation, Formal analysis, Data

curation, Conceptualization. **Patricia Yuste-Checa:** Writing – review & editing, Resources, Methodology. **Fatemeh Mamashli:** Writing – review & editing, Visualization, Methodology, Investigation. **Matthias Schmitz:** Writing – review & editing, Visualization, Investigation, Formal analysis, Data curation. **Maria Georgina Herrera:** Writing – review & editing, Visualization, Methodology, Investigation, Formal analysis. **Susana Margarida da Silva Correia:** Investigation, Data curation. **Kalpshree Gogte:** Methodology, Investigation, Data curation. **Verian Bader:** Methodology, Formal analysis. **Inga Zerr:** Writing – review & editing, Methodology, Funding acquisition. **F. Ulrich Hartl:** Writing – review & editing, Funding acquisition, Conceptualization. **Andreas Bracher:** Writing – review & editing, Resources, Methodology, Conceptualization. **Konstanze F. Winklhofer:** Writing – review & editing, Writing – original draft, Conceptualization. **Jörg Tatzelt:** Writing – review & editing, Writing – original draft, Funding acquisition, Conceptualization.

Funding

This work was funded by the Deutsche Forschungsgemeinschaft (DFG, German Research Foundation) under Germany's Excellence Strategy – EXC 2033 – 390677874 – RESOLV; TA 167/6-3 and TA 167/11-1 (to JT); WI/2111-6 (to KFW).

Confocal laser scanning and SR-SIM microscopy was funded by the German Research Foundation and the State Government of North Rhine-Westphalia (INST 213/840-1 FUGG).

DATA AVAILABILITY

All data are contained within the manuscript and the supplementary figures.

DECLARATION OF COMPETING INTEREST

The authors declare that they have no known competing financial interests or personal relationships that could have appeared to influence the work reported in this paper.

Acknowledgments

We are grateful to Petra Goldmann and Andrea Roth-Sturm for technical support.

Appendix A. Supplementary material

Supplementary material to this article can be found online at https://doi.org/10.1016/j.jmb.2024.168839.

Received 7 June 2024;
Accepted 23 October 2024;
Available online 28 October 2024

Keywords:
liquid–liquid phase separation;
neurodegeneration;
prion;
chaperone;
clusterin

AbbreviationsLLPS, liquid–liquid phase separation; PrP, prion protein; CJD, Creutzfeldt-Jakob disease; TEV, tobacco etch virus

References

1. Prusiner, S.B., (1998). Prions. *PNAS* **95**, 13363–13383.
2. Chen, S.G., Teplow, D.B., Parchi, P., Teller, J.K., Gambetti, P., Autilio-Gambetti, L., (1995). Truncated forms of the human prion protein in normal brain and in prion diseases. *J. Biol. Chem.* **270**, 19173–19180.
3. Mange, A., Beranger, F., Peoc'h, K., Onodera, T., Frobert, Y., Lehmann, S., (2004). Alpha- and beta- cleavages of the amino-terminus of the cellular prion protein. *Biol. Cell* **96**, 125–132.
4. Harris, D.A., Huber, M.T., van Dijken, P., Shyng, S.L., Chait, B.T., Wang, R., (1993). Processing of a cellular prion protein: identification of N- and C-terminal cleavage sites. *Biochemistry* **32**, 1009–1016.
5. Altmeppen, H.C., Puig, B., Dohler, F., Thurm, D.K., Falker, C., Krasemann, S., et al., (2012). Proteolytic processing of the prion protein in health and disease. *Am. J. Neurodegener. Dis.* **1**, 15–31.
6. Laffont-Proust, I., Faucheux, B.A., Hassig, R., Sazdovitch, V., Simon, S., Grassi, J., et al., (2005). The N-terminal cleavage of cellular prion protein in the human brain. *FEBS Lett.* **579**, 6333–6337.
7. Shyng, S.L., Huber, M.T., Harris, D.A., (1993). A prion protein cycles between the cell surface and an endocytic compartment in cultured neuroblastoma cells. *J. Biol. Chem.* **268**, 15922–15928.
8. Castle, A.R., Kang, S.G., Eskandari-Sedighi, G., Wohlgemuth, S., Nguyen, M.A., Drucker, D.J., et al., (2023). Beta-endoproteolysis of the cellular prion protein by dipeptidyl peptidase-4 and fibroblast activation protein. *PNAS* **120**, e2209815120
9. Tange, H., Ishibashi, D., Nakagaki, T., Taguchi, Y., Kamatari, Y.O., Ozawa, H., et al., (2021). Liquid-liquid phase separation of full-length prion protein initiates conformational conversion in vitro. *J. Biol. Chem.* 100367.
10. Huang, J.J., Li, X.N., Liu, W.L., Yuan, H.Y., Gao, Y., Wang, K., et al., (2020). Neutralizing mutations significantly inhibit amyloid formation by human prion protein and decrease its cytotoxicity. *J. Mol. Biol.* **432**, 828–844.
11. Matos, C.O., Passos, Y.M., do Amaral, M.J., Macedo, B., Tempone, M.H., Bezerra, O.C.L., et al., (2020). Liquid-liquid phase separation and fibrillation of the prion protein modulated by a high-affinity DNA aptamer. *FASEB J.* **34**, 365–385.
12. Kostylev, M.A., Tuttle, M.D., Lee, S., Klein, L.E., Takahashi, H., Cox, T.O., et al., (2018). Liquid and hydrogel phases of PrP(C) linked to conformation shifts

and triggered by Alzheimer's amyloid-beta oligomers. *Mol. Cell* **72**, 426–443.e12.
13. Passos, Y.M., do Amaral, M.J., Ferreira, N.C., Macedo, B., Chaves, J.A.P., de Oliveira, V.E., et al., (2021). The interplay between a GC-rich oligonucleotide and copper ions on prion protein conformational and phase transitions. *Int. J. Biol. Macromol.* **173**, 34–43.
14. Kamps, J., Lin, Y.H., Oliva, R., Bader, V., Winter, R., Winklhofer, K.F., et al., (2021). The N-terminal domain of the prion protein is required and sufficient for liquid-liquid phase separation: A crucial role of the Abeta-binding domain. *J. Biol. Chem.* **297**, 100860
15. Agarwal, A., Rai, S.K., Avni, A., Mukhopadhyay, S., (2021). An intrinsically disordered pathological prion variant Y145Stop converts into self-seeding amyloids via liquid-liquid phase separation. *PNAS* **118**
16. Polido, S.A., Stuani, C., Voigt, A., Banik, P., Kamps, J., Bader, V., et al., (2024). Cross-seeding by prion protein inactivates TDP-43. *Brain* **147**, 240–254.
17. Ramos, S., Kamps, J., Pezzotti, S., Winklhofer, K.F., Tatzelt, J., Havenith, M., (2023). Hydration makes a difference! How to tune protein complexes between liquid-liquid and liquid-solid phase separation. *PCCP* **25**, 28063–28069.
18. Alberti, S., Dormann, D., (2019). Liquid-liquid phase separation in disease. *Annu. Rev. Genet.* **53**, 171–194.
19. Babinchak, W.M., Surewicz, W.K., (2020). Liquid-liquid phase separation and its mechanistic role in pathological protein aggregation. *J. Mol. Biol.* **432**, 1910–1925.
20. Darling, A.L., Shorter, J., (2021). Combating deleterious phase transitions in neurodegenerative disease. *Biochim. Biophys. Acta* **1868**, 118984
21. Zbinden, A., Perez-Berlanga, M., De Rossi, P., Polymenidou, M., (2020). Phase separation and neurodegenerative diseases: A disturbance in the force. *Dev. Cell* **55**, 45–68.
22. Chen, Y., Cohen, T.J., (2019). Aggregation of the nucleic acid-binding protein TDP-43 occurs via distinct routes that are coordinated with stress granule formation. *J. Biol. Chem.* **294**, 3696–3706.
23. Hans, F., Glasebach, H., Kahle, P.J., (2020). Multiple distinct pathways lead to hyperubiquitylated insoluble TDP-43 protein independent of its translocation into stress granules. *J. Biol. Chem.* **295**, 673–689.
24. Ratti, A., Gumina, V., Lenzi, P., Bossolasco, P., Fulceri, F., Volpe, C., et al., (2020). Chronic stress induces formation of stress granules and pathological TDP-43 aggregates in human ALS fibroblasts and iPSC-motoneurons. *Neurobiol. Dis.* **145**, 105051
25. Cascella, R., Bigi, A., Riffert, D.G., Gagliani, M.C., Ermini, E., Moretti, M., et al., (2022). A quantitative biology approach correlates neuronal toxicity with the largest inclusions of TDP-43. *Sci. Adv.* **8**, eabm6376
26. Sternburg, E.L., Gruijs da Silva, L.A., Dormann, D., (2022). Post-translational modifications on RNA-binding proteins: accelerators, brakes, or passengers in neurodegeneration? *Trends Biochem. Sci.* **47**, 6–22.
27. Snead, W.T., Gladfelter, A.S., (2019). The Control centers of biomolecular phase separation: How membrane surfaces, PTMs, and active processes regulate condensation. *Mol. Cell* **76**, 295–305.
28. Satapathy, S., Wilson, M.R., (2021). The dual roles of clusterin in extracellular and intracellular proteostasis. *Trends Biochem. Sci* **46**, 652–660.
29. Wilson, M.R., Satapathy, S., Vendruscolo, M., (2023). Extracellular protein homeostasis in neurodegenerative diseases. *Nature Rev. Neurol.* **19**, 235–245.
30. Narayan, P., Orte, A., Clarke, R.W., Bolognesi, B., Hook, S., Ganzinger, K.A., et al., (2011). The extracellular chaperone clusterin sequesters oligomeric forms of the amyloid-beta(1–40) peptide. *Nature Struct. Mol. Biol.* **19**, 79–83.
31. Wyatt, A.R., Yerbury, J.J., Ecroyd, H., Wilson, M.R., (2013). Extracellular chaperones and proteostasis. *Annu. Rev. Biochem* **82**, 295–322.
32. Whiten, D.R., Cox, D., Horrocks, M.H., Taylor, C.G., De, S., Flagmeier, P., et al., (2018). Single-molecule characterization of the interactions between extracellular chaperones and toxic alpha-synuclein oligomers. *Cell Rep.* **23**, 3492–3500.
33. Poon, S., Easterbrook-Smith, S.B., Rybchyn, M.S., Carver, J.A., Wilson, M.R., (2000). Clusterin is an ATP-independent chaperone with very broad substrate specificity that stabilizes stressed proteins in a folding-competent state. *Biochemistry* **39**, 15953–15960.
34. Yuste-Checa, P., Trinkaus, V.A., Riera-Tur, I., Imamoglu, R., Schaller, T.F., Wang, H., et al., (2021). The extracellular chaperone Clusterin enhances Tau aggregate seeding in a cellular model. *Nature Commun.* **12**, 4863.
35. Mok, S.A., Condello, C., Freilich, R., Gillies, A., Arhar, T., Oroz, J., et al., (2018). Mapping interactions with the chaperone network reveals factors that protect against tau aggregation. *Nature Struct. Mol. Biol.* **25**, 384–393.
36. Scheidt, T., Lapinska, U., Kumita, J.R., Whiten, D.R., Klenerman, D., Wilson, M.R., et al., (2019). Secondary nucleation and elongation occur at different sites on Alzheimer's amyloid-beta aggregates. *Sci. Adv.* **5**, eaau3112
37. Sasaki, K., Doh-ura, K., Ironside, J.W., Iwaki, T., (2002). Increased clusterin (apolipoprotein J) expression in human and mouse brains infected with transmissible spongiform encephalopathies. *Acta Neuropathol.* **103**, 199–208.
38. Chiesa, R., Angeretti, N., Lucca, E., Salmona, M., Tagliavini, F., Bugiani, O., et al., (1996). Clusterin (SGP-2) induction in rat astroglial cells exposed to prion protein fragment 106–126. *Eur. J. Neurosci.* **8**, 589–597.
39. Freixes, M., Puig, B., Rodriguez, A., Torrejon-Escribano, B., Blanco, R., Ferrer, I., (2004). Clusterin solubility and aggregation in Creutzfeldt-Jakob disease. *Acta Neuropathol.* **108**, 295–301.
40. Kempster, S., Collins, M.E., Aronow, B.J., Simmons, M., Green, R.B., Edington, N., (2004). Clusterin shortens the incubation and alters the histopathology of bovine spongiform encephalopathy in mice. *Neuroreport* **15**, 1735–1738.
41. Hofweber, M., Hutten, S., Bourgeois, B., Spreitzer, E., Niedner-Boblenz, A., Schifferer, M., et al., (2018). Phase separation of FUS is suppressed by its nuclear import receptor and arginine methylation. *Cell* **173**, 706–719.e13.
42. Wegmann, S., Eftekharzadeh, B., Tepper, K., Zoltowska, K.M., Bennett, R.E., Dujardin, S., et al., (2018). Tau protein liquid-liquid phase separation can initiate tau aggregation. *EMBO J.* **37**
43. Saito, M., Hess, D., Eglinger, J., Fritsch, A.W., Kreysing, M., Weinert, B.T., et al., (2019). Acetylation of intrinsically disordered regions regulates phase separation. *Nature Chem. Biol.* **15**, 51–61.

44. Goel, S., Oliva, R., Jeganathan, S., Bader, V., Krause, L.J., Kriegler, S., et al., (2023). Linear ubiquitination induces NEMO phase separation to activate NF-kappaB signaling. *Life Sci. Alliance* **6**
45. Dao, T.P., Kolaitis, R.M., Kim, H.J., O'Donovan, K., Martyniak, B., Colicino, E., et al., (2018). Ubiquitin modulates liquid-liquid phase separation of UBQLN2 via disruption of multivalent interactions. *Mol. Cell* **69**, 965–978.e6.
46. Ren, J., Wang, S., Zong, Z., Pan, T., Liu, S., Mao, W., et al., (2024). TRIM28-mediated nucleocapsid protein SUMOylation enhances SARS-CoV-2 virulence. *Nature Commun.* **15**, 244.
47. Rhine, K., Dasovich, M., Yoniles, J., Badiee, M., Skanchy, S., Ganser, L.R., et al., (2022). Poly(ADP-ribose) drives condensation of FUS via a transient interaction. *Mol. Cell* **82**, 969–985.e11.
48. Banik, P., Ray, K., Kamps, J., Chen, Q.Y., Luesch, H., Winklhofer, K.F., et al., (2024). VCP/p97 mediates nuclear targeting of non-ER-imported prion protein to maintain proteostasis. *Life Sci. Alliance* **7**
49. Kamps, J., Bader, V., Winklhofer, K.F., Tatzelt, J., (2024). Liquid-liquid phase separation of the prion protein is regulated by the octarepeat domain independently of histidines and copper. *J. Biol. Chem.* **300**, 107310
50. Bolder, S.G., Sagis, L.M., Venema, P., van der Linden, E., (2007). Thioflavin T and birefringence assays to determine the conversion of proteins into fibrils. *Langmuir* **23**, 4144–4147.
51. Resenberger, U.K., Muller, V., Munter, L.M., Baier, M., Multhaup, G., Wilson, M.R., et al., (2012). The heat shock response is modulated by and interferes with toxic effects of scrapie prion protein and amyloid beta. *J. Biol. Chem.* **287**, 43765–43776.
52. Yerbury, J.J., Poon, S., Meehan, S., Thompson, B., Kumita, J.R., Dobson, C.M., et al., (2007). The extracellular chaperone clusterin influences amyloid formation and toxicity by interacting with prefibrillar structures. *FASEB J.* **21**, 2312–2322.
53. West, J., Satapathy, S., Whiten, D.R., Kelly, M., Geraghty, N.J., Proctor, E.J., et al., (2021). Neuroserpin and transthyretin are extracellular chaperones that preferentially inhibit amyloid formation. *Sci. Adv.* **7**, eabf7606
54. Schmitt-Ulms, G., Hansen, K., Liu, J., Cowdrey, C., Yang, J., DeArmond, S.J., et al., (2004). Time-controlled transcardiac perfusion cross-linking for the study of protein interactions in complex tissues. *Nature Biotechnol.* **22**, 724–731.
55. Xu, F., Karnaukhova, E., Vostal, J.G., (2008). Human cellular prion protein interacts directly with clusterin protein. *Biochim. Biophys. Acta* **1782**, 615–620.
56. Prusiner, S.B., Scott, M., Foster, D., Pan, K.-M., Groth, D., Mirenda, C., et al., (1990). Transgenetic studies implicate interactions between homologous PrP isoforms in scrapie prion replication. *Cell* **63**, 673–686.
57. Atarashi, R., Wilham, J.M., Christensen, L., Hughson, A. G., Moore, R.A., Johnson, L.M., et al., (2008). Simplified ultrasensitive prion detection by recombinant PrP conversion with shaking. *Nature Methods* **5**, 211–212.
58. Neumann, M., Sampathu, D.M., Kwong, L.K., Truax, A.C., Micsenyi, M.C., Chou, T.T., et al., (2006). Ubiquitinated TDP-43 in frontotemporal lobar degeneration and amyotrophic lateral sclerosis. *Science* **314**, 130–133.
59. Baba, M., Nakajo, S., Tu, P.H., Tomita, T., Nakaya, K., Lee, V.M., et al., (1998). Aggregation of alpha-synuclein in Lewy bodies of sporadic Parkinson's disease and dementia with Lewy bodies. *Am. J. Pathol.* **152**, 879–884.
60. DiFiglia, M., Sapp, E., Chase, K.O., Davies, S.W., Bates, G.P., Vonsattel, J.P., et al., (1997). Aggregation of huntingtin in neuronal intranuclear inclusions and dystrophic neurites in brain. *Science* **277**, 1990–1993.
61. Schneider, M.M., Gautam, S., Herling, T.W., Andrzejewska, E., Krainer, G., Miller, A.M., et al., (2021). The Hsc70 disaggregation machinery removes monomer units directly from alpha-synuclein fibril ends. *Nature Commun.* **12**, 5999.
62. Ahlers, J., Adams, E.M., Bader, V., Pezzotti, S., Winklhofer, K.F., Tatzelt, J., et al., (2021). The key role of solvent in condensation: mapping water in liquid-liquid phase-separated FUS. *Biophys. J.* **120**, 1266–1275.
63. Furthmann, N., Bader, V., Angersbach, L., Blusch, A., Goel, S., Sanchez-Vicente, A., et al., (2023). NEMO reshapes the alpha-Synuclein aggregate interface and acts as an autophagy adapter by co-condensation with p62. *Nature Commun.* **14**, 8368.
64. Schmitz, M., Cramm, M., Llorens, F., Muller-Cramm, D., Collins, S., Atarashi, R., et al., (2016). The real-time quaking-induced conversion assay for detection of human prion disease and study of other protein misfolding diseases. *Nature Protoc.* **11**, 2233–2242.
65. Cramm, M., Schmitz, M., Karch, A., Mitrova, E., Kuhn, F., Schroeder, B., et al., (2016). Stability and reproducibility underscore utility of RT-QuIC for diagnosis of Creutzfeldt-Jakob disease. *Mol. Neurobiol.* **53**, 1896–1904.
66. Orru, C.D., Wilham, J.M., Raymond, L.D., Kuhn, F., Schroeder, B., Raeber, A.J., et al., (2011). Prion disease blood test using immunoprecipitation and improved quaking-induced conversion. *MBio* **2**, e00078-11